JOURNAL OF Applied Polymer SCIENCE

Special Issue: Microfiltration and Ultrafiltration Membrane Science and Technology

Guest Editors: Prof. Isabel C. Escobar (University of Toledo) and Prof. Bart Van der Bruggen (University of Leuven)

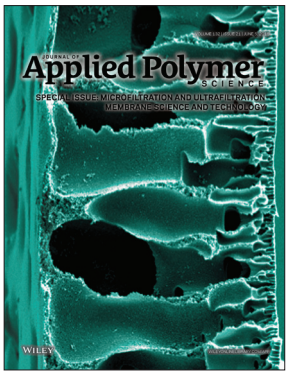

EDITORIAL

Microfiltration and Ultrafiltration Membrane Science and Technology
I. C. Escobar and B. Van der Bruggen, *J. Appl. Polym. Sci.* 2015, **DOI: 10.1002/app.42002**

REVIEWS

Nanoporous membranes generated from self-assembled block polymer precursors: *Quo Vadis*?
Y. Zhang, J. L. Sargent, B. W. Boudouris and W. A. Phillip, *J. Appl. Polym. Sci.* 2015, **DOI: 10.1002/app.41683**

Making polymeric membranes anti-fouling via "grafting from" polymerization of zwitterions
Q. Li, J. Imbrogno, G. Belfort and X.-L. Wang, *J. Appl. Polym. Sci.* 2015, **DOI: 10.1002/app.41781**

Fouling control on MF/ UF membranes: Effect of morphology, hydrophilicity and charge
R. Kumar and A. F. Ismail, *J. Appl. Polym. Sci.* 2015, **DOI: 10.1002/app.42042**

EMERGING MATERIALS AND FABRICATION

Preparation of a poly(phthalazine ether sulfone ketone) membrane with propanedioic acid as an additive and the prediction of its structure
P. Qin, A. Liu and C. Chen, *J. Appl. Polym. Sci.* 2015, **DOI: 10.1002/app.41621**

Preparation and characterization of MOF-PES ultrafiltration membranes
L. Zhai, G. Li, Y. Xu, M. Xiao, S. Wang and Y. Meng, *J. Appl. Polym. Sci.* 2015, **DOI: 10.1002/app.41663**

Tailoring of structures and permeation properties of asymmetric nanocomposite cellulose acetate/silver membranes
A. S. Figueiredo, M. G. Sánchez-Loredo, A. Maurício, M. F. C. Pereira, M. Minhalma and M. N. de Pinho, *J. Appl. Polym. Sci.* 2015, **DOI: 10.1002/app.41796**

LOW-FOULING POLYMERS

Low fouling polysulfone ultrafiltration membrane via click chemistry
Y. Xie, R. Tayouo and S. P. Nunes, *J. Appl. Polym. Sci.* 2015, **DOI: 10.1002/app.41549**

Elucidating membrane surface properties for preventing fouling of bioreactor membranes by surfactin
N. Behary, D. Lecouturier, A. Perwuelz and P. Dhulster, *J. Appl. Polym. Sci.* 2015, **DOI: 10.1002/app.41622**

PVC and PES-*g*-PEGMA blend membranes with improved ultrafiltration performance and fouling resistance
S. Jiang, J. Wang, J. Wu and Y. Chen, *J. Appl. Polym. Sci.* 2015, **DOI: 10.1002/app.41726**

Improved antifouling properties of TiO_2/PVDF nanocomposite membranes in UV coupled ultrafiltration
M. T. Moghadam, G. Lesage, T. Mohammadi, J.-P. Mericq, J. Mendret, M. Heran, C. Faur, S. Brosillon, M. Hemmati and F. Naeimpoor, *J. Appl. Polym. Sci.* 2015, **DOI: 10.1002/app.41731**

Development of functionalized doped carbon nanotube/polysulfone nanofiltration membranes for fouling control
P. Xie, Y. Li and J. Qiu, *J. Appl. Polym. Sci.* 2015, **DOI: 10.1002/app.41835**

JOURNAL OF Applied Polymer SCIENCE

Special Issue: Microfiltration and Ultrafiltration Membrane Science and Technology

Guest Editors: Prof. Isabel C. Escobar (University of Toledo) and
Prof. Bart Van der Bruggen (University of Leuven)

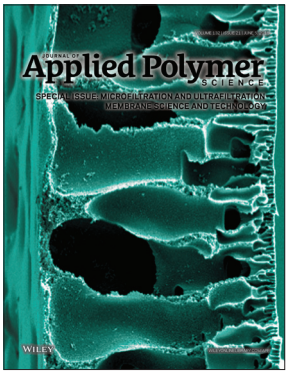

SURFACE MODIFICATION OF POLYMER MEMBRANES

Highly chlorine and oily fouling tolerant membrane surface modifications by *in situ* polymerization of dopamine and poly(ethylene glycol) diacrylate for water treatment
K. Yokwana, N. Gumbi, F. Adams, S. Mhlanga, E. Nxumalo and B. Mamba, *J. Appl. Polym. Sci.* 2015, **DOI: 10.1002/app.41661**

Fouling control through the hydrophilic surface modification of poly(vinylidene fluoride) membranes
H. Jang, D.-H. Song, I.-C. Kim, and Y.-N. Kwon, *J. Appl. Polym. Sci.* 2015, **DOI: 10.1002/app.41712**

Hydroxyl functionalized PVDF-TiO_2 ultrafiltration membrane and its antifouling properties
Y. H. Teow, A. A. Latif, J. K. Lim, H. P. Ngang, L. Y. Susan and B. S. Ooi, *J. Appl. Polym. Sci.* 2015, **DOI: 10.1002/app.41844**

Enhancing the antifouling properties of polysulfone ultrafiltration membranes by the grafting of poly(ethylene glycol) derivatives via surface amidation reactions
H. Yu, Y. Cao, G. Kang, Z. Liu, W. Kuang, J. Liu and M. Zhou, *J. Appl. Polym. Sci.* 2015, **DOI: 10.1002/app.41870**

SEPARATION APPLICATIONS

Experiment and simulation of the simultaneous removal of organic and inorganic contaminants by micellar enhanced ultrafiltration with mixed micelles
A. D. Vibhandik, S. Pawar and K. V. Marathe, *J. Appl. Polym. Sci.* 2015, **DOI: 10.1002/app.41435**

Polymeric membrane modification using SPEEK and bentonite for ultrafiltration of dairy wastewater
A. Pagidi, Y. Lukka Thuyavan, G. Arthanareeswaran, A. F. Ismail, J. Jaafar and D. Paul, *J. Appl. Polym. Sci.* 2015, **DOI: 10.1002/app.41651**

Forensic analysis of degraded polypropylene hollow fibers utilized in microfiltration
X. Lu, P. Shah, S. Maruf, S. Ortiz, T. Hoffard and J. Pellegrino, *J. Appl. Polym. Sci.* 2015, **DOI: 10.1002/app.41553**

A surface-renewal model for constant flux cross-flow microfiltration
S. Jiang and S. G. Chatterjee, *J. Appl. Polym. Sci.* 2015, **DOI: 10.1002/app.41778**

Ultrafiltration of aquatic humic substances through magnetically responsive polysulfone membranes
N. A. Azmi, Q. H. Ng and S. C. Low, *J. Appl. Polym. Sci.* 2015, **DOI: 10.1002/app.41874**

BIOSEPARATIONS APPLICATIONS

Analysis of the effects of electrostatic interactions on protein transport through zwitterionic ultrafiltration membranes using protein charge ladders
M. Hadidi and A. L. Zydney, *J. Appl. Polym. Sci.* 2015, **DOI: 10.1002/app.41540**

Modification of microfiltration membranes by hydrogel impregnation for pDNA purification
P. H. Castilho, T. R. Correia, M. T. Pessoa de Amorim, I. C. Escobar, J. A. Queiroz, I. J. Correia and A. M. Morão, *J. Appl. Polym. Sci.* 2015, **DOI: 10.1002/app.41610**

Hemodialysis membrane surface chemistry as a barrier to lipopolysaccharide transfer
B. Madsen, D. W. Britt, C.-H. Ho, M. Henrie, C. Ford, E. Stroup, B. Maltby, D. Olmstead and M. Andersen, *J. Appl. Polym. Sci.* 2015, **DOI: 10.1002/app.41550**

Membrane adsorbers comprising grafted glycopolymers for targeted lectin binding
H. C. S. Chenette and S. M. Husson, *J. Appl. Polym. Sci.* 2015, **DOI: 10.1002/app.41437**

Journal of Applied Polymer Science

Hydroxyl functionalized PVDF-TiO_2 ultrafiltration membrane and its antifouling properties

Yeit Haan Teow, Ahmad Abdul Latif, Jit Kang Lim, Huey Ping Ngang, Ling Ying Susan, Boon Seng Ooi

School of Chemical Engineering, Engineering Campus, Universiti Sains Malaysia, Seri Ampangan, 14300 Nibong Tebal, Penang, Malaysia

Correspondence to: B. S. Ooi (E-mail: chobs@usm.my)

ABSTRACT: In this study, polyvinylidene fluoride (PVDF) was hydroxylized via the Fenton reaction and was used as a polymer matrix for mixed-matrix membrane synthesis. The chemical properties of hydroxylized PVDF (PVDF–OH) polymer and pristine PVDF polymer were investigated by Fourier transform infrared spectroscopy (FTIR). Treatment of PVDF polymer with Fenton reagent led to the emergence of the OH functionality. The field emission scanning electron microscope (FESEM) and energy dispersive X-ray (EDX) analysis clearly indicated the improvement of titanium dioxide (TiO_2) nanoparticles (NPs) distribution on the PVDF–OH/TiO_2 mixed-matrix membrane (MMM) surface. The antifouling properties of the neat PVDF membrane, PVDF/TiO_2 MMM and PVDF–OH/TiO_2 MMM were investigated. The MMM with the embedded P25 TiO_2 was found to show better antifouling ability, with a considerably higher irreversible flux recovery ratio after 6 h of UV irradiation. By hydroxylizing the PVDF matrix, the TiO_2 NP dispersion was improved. The PVDF–OH/TiO_2 MMM combined both the superior antifouling and UV-cleaning properties. © 2015 Wiley Periodicals, Inc. J. Appl. Polym. Sci. **2015**, *132*, 41844.

KEYWORDS: composites; functionalization of polymers; membranes; nanoparticles; nanowires and nanocrystals

Received 2 August 2014; accepted 8 December 2014

DOI: 10.1002/app.41844

INTRODUCTION

Polyvinylidene fluoride (PVDF) is a semi-crystalline polymer that has been used extensively in membrane fabrication because of its excellent chemical resistance to aggressive reagents,[1] flexibility, excellent thermal stability, UV stability, good mechanical strength, and membrane forming properties compared to other commercial polymers.[2–6] These properties make PVDF an ideal membrane material for various wastewater treatment applications.[5,7,8] Unfortunately, the inherent hydrophobic nature of the PVDF membrane often limits its application as the PVDF membrane exhibits a lower permeation flux due to the high surface tension between water and the membrane surface. A hydrophobic membrane is susceptible to severe fouling problems, a property that has become a conspicuous drawback for the application of these membranes in water treatment.

Recent advances in nanotechnology have greatly expanded the avenues of membrane modification by introducing nanoparticles (NPs) for functionalizing the membrane[9–12] to improve the synergetic effects on water and wastewater treatment.[9] Because of its unique large surface-to-volume ratio and strong reactivity, nano-sized TiO_2 particles have emerged as a highly promising material to be incorporated into the polymeric matrix as a hydrophilic filler.[13,14] Bae and Tak,[15] Yu *et al.*,[16] Li *et al.*,[12] and Rahimpour *et al.*[17] have demonstrated that the mixed-matrix membrane (MMM) can provide the fouling-resistance to the neat polymeric membrane by immobilizing the TiO_2 NPs. In addition to this passive defouling mechanism, a more dynamic fouling mitigation effect could also be achieved by incorporating the photocatalytic NPs to create a membrane with self-cleaning properties.

In our previous study, efforts were devoted to the preparation of a mixed-matrix ultrafiltration (UF) membrane using a method that involves simultaneous phase inversion and embedding of particles.[18] Although previous study had shown that the TiO_2 dispersion and size were affected by the size of the TiO_2 particles prepared in the coagulation bath, the high surface energy between the NPs and the polymer matrix often resulted in avoidable particle agglomeration. This particle agglomeration led to a low functional surface area and high surface roughness.[19] Many studies have attempted to improve dispersion by coating the TiO_2 with a low surface energy material or by adding a dispersant. However, the coating process might impair the TiO_2 photocatalytic behavior. A more feasible approach to the synthesis of ultrafine and well dispersed TiO_2 NPs in a polymer matrix is therefore desirable.

In this work, high surface tension between the NPs and the polymer matrix were overcome by partially hydroxylizing the PVDF polymer via the Fenton reaction. The Fenton reaction was followed by the embedment of TiO_2 particles via simultaneous solvent exchange and phase inversion in a colloidal stable suspension bath. The resulting OH functional group on the PVDF–OH polymer matrix was expected to promote stronger interactions with the fine NPs and PVDF–OH to improve the distribution, lower surface roughness (low fouling) and promote a higher reactive surface area (better UV-cleaning).

EXPERIMENTAL

Materials

UF flat sheet membranes were fabricated by dissolving PVDF (TA6010/1001, Solvay Solexis, Shanghai) in *N*-*N*-dimethylacetamide (DMAc) (Merck, Germany) [assay (GC, area %) $\geq$ 99%] solution and were cast at 200 μm thickness. The commercial TiO_2 nanopowder was purchased from Sigma-Aldrich, St. Louis, MO (trade name: P25; particle size $\sim$ 21 nm). As reported by the manufacturer, P25 contains approximately 75% anatase and 25% rutile. The NPs were used as received.

Anhydrous ethanol (C_2H_5OH), hydrogen peroxide (H_2O_2), iron (II) sulfate heptahydrate, ($FeSO_4{\cdot}7H_2O$), and sulfuric acid (H_2SO_4) were the Fenton reagents used to prepare hydroxyl-functionalized PVDF polymer and were all supplied by Merck, Germany. Synthetic humic acid (HA) with a molecular weight range of 20,000-50,000 g/mol was obtained from Sigma-Aldrich and used as the organic foulant during the experiment without further purification. Sodium hydroxide, NaOH (Sigma-Aldrich, USA) solution was used to improve the dissolution of HA in water.

For the adsorption study, feed solutions were prepared by dissolving 20 mg of pre-weighed HA powder in 1 L of distilled water. For the effect of HA fouling, feed solutions were prepared by dissolving 10 mg of pre-weighed HA powder in 5 L of distilled water. The solution pH was adjusted to pH 7 by the addition of a small quantity of 0.1*M* NaOH with vigorous stirring. Analytical grade anhydrous calcium chloride ($CaCl_2$, 1 m*M*) (R & M Chemicals, UK) was added to adjust the total ionic strength of the HA feed solution.

Synthesis of Hydroxyl-Functionalized PVDF Polymer

PVDF–OH polymer was synthesized by a Fenton reaction, in which 18 g of PVDF, 2.502 g of $FeSO_4{\cdot}7H_2O$ (900 mmol), 0.738 g of H_2O_2 (10.8 mol), 90 mL of C_2H_5OH and 90 mL of deionized water were reacted for 1 h in a flask controlled at 50°C using a water bath. The resulting product was filtered and washed thoroughly with excess sulfuric acid (H_2SO_4) and water to remove the Fe^{3+} salt adsorbed on the polymer (Figure 1). The polymer was then dried overnight in an oven at 70°C. The mechanism of hydroxylation is shown below:

$$Fe^{2+} + H_2O_2 \rightarrow Fe^{3+} + HO\bullet + OH^- \quad (1)$$

$$Fe^{3+} + H_2O_2 \rightarrow Fe^{2+} + HOO\bullet + H^+ \quad (2)$$

Preparation of Stable TiO_2 Colloid Suspension

Chemical and mechanical methods were used to prepare the TiO_2 colloidal suspension that was used as a coagulation bath

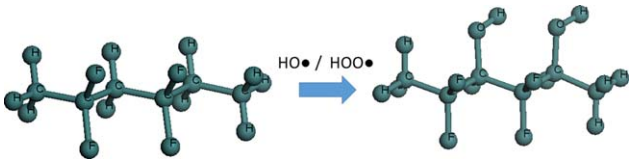

Figure 1. Mechanism of PVDF hydroxylation. [Color figure can be viewed in the online issue, which is available at wileyonlinelibrary.com.]

for the membrane phase inversion. The chemical modification was carried out first, followed by application of the mechanical method as described in our previous report.[18–20] In brief, the pH value of the TiO_2 suspension was adjusted until the pH reached equilibrium at pH 4.0 to achieve electrostatic stability (zeta potential $>\pm$ 30 mV) with an average hydrodynamic cluster size of 200 nm in suspension, as reported in our previous study.[19,21] When the zeta potential value is less than -30 mV or greater than $+30$ mV, particles in suspensions tend to repel each other, and therefore, no agglomeration occurs. To further break the agglomerated TiO_2 cluster, the TiO_2 suspension was subjected to 15 min of ultrasonic irradiation. The colloidal stability was evaluated based on the zeta potential and particle size distribution (apparent hydrodynamic size) of TiO_2 NPs using a Malvern Zetasizer Nano NS90 (Malvern Instruments, United Kingdom) on the basis of DLS theory and the cumulative method. The measurements were carried out using a clear disposable zeta cell at 25°C, with the TiO_2 refractive index (RI) and absorption set at 2.500 and 0.10.[22,23] Water was chosen as the dispersant for the measurement with a viscosity of 0.8872 cP and a RI of 1.330. The reported values were taken from three measurements of 15 runs and 20 runs for TiO_2 particle size distribution and zeta potential, respectively, to minimize analytical error.

Membrane Formation and *In Situ* Particle Embedment

The membrane casting solutions were prepared by dissolving pre-dried PVDF polymer or PVDF–OH polymer (24 h of oven drying at 70°C) using DMAc in a 200 mL beaker. The composition of the PVDF/DMAc was maintained at a weight percentage ratio of 18: 82.

The mixture was subjected to an initial constant stirring of 250 rpm at 65°C for 4 h to form a homogeneous solution. The homogenous membrane polymer solution was then left overnight with stirring at 40°C and then kept in a centrifuge tube. The trapped air bubbles were removed by allowing the solution to stand overnight. Solvent loss by evaporation was negligible due to the high boiling point of DMAc of 164–166°C.

The polymer solution was cast using a thin film applicator (Elcometer 4340, Elcometer (Asia) Pte.) on a flat glass plate wrapped with non-woven polyester fabric (Holleytex 3329, Ahlstrom) to form a film at a nominal thickness of 200 μm. The polyester fabric acts as a membrane support layer, providing mechanical strength to the membrane for pressure resistance. Thereafter, the nascent membrane on the glass plate was solidified by immediate immersion into a coagulation bath consists of either distilled water or TiO_2 suspension at room temperature (26°C) to avoid excessive surface evaporation. The immersion was left for a day to ensure complete solidification and

removal of residual solvent from the membranes. The resulting fabricated membrane was then recovered from the coagulation bath after detaching the membrane from the glass plate, with subsequent rinsing with distilled water and soaking in a bath of fresh distilled water. Drying was done after dipping the membrane in ethanol to avoid microbial growth.

TiO_2 particles were introduced onto the membrane matrix by immersing the nascent PVDF or PVDFOH membrane on the glass plate into the prepared 0.01 g/L TiO_2 colloidal suspension. Because the membrane surface solidification and NP embedment occur simultaneously, this NP incorporation method is an *in-situ* approach.

Membrane Characterization

Fourier Transform Infrared (FTIR) Spectroscopy. Fourier Transform Infrared (FTIR) spectra of the PVDF and PVDF–OH polymer were obtained to investigate the functional groups on the polymer surface. The FTIR (FTIR, Nicolet Nexus 670, USA) was equipped with an OMNI-sample attenuated total reflection (ATR) smart accessory and was coupled to a diamond crystal operated at an incidence angle of 45°. Each of the spectra was recorded as the average of 32 scans taken with a resolution of 4 cm^{-1} and was collected at an operating wave number ranging from 4000 to 425 cm^{-1}. The pressure was equal in all samples to avoid differences caused by the different penetrating depth.

Membrane Pore Size Distribution. Pore size of the membranes was determined using gas flow/liquid displacement method via Capillary Flow Porometer Porolux 1000 (CNG Instruments). Membrane samples with diameter of 10 mm were characterized using the "dry up-wet up" method. In this method, gas flow was measured as a function of transmembrane pressure, through wetted membrane with 1,1,2,3,3,3-haxafluoropropene and the dried membrane. The pore size distribution was estimated using PMI software.

FESEM and EDX Analysis. The surface morphology of the synthesized PVDF/TiO_2 MMM and PVDF–OH/TiO_2 MMM was probed using a field emission scanning electron microscope (FESEM) (SUPRA 35 VP, Carl Zeiss Inc.). For the FESEM observation, the membranes were initially immersed in C_2H_5OH for a few seconds, dried with a filter paper to remove the remaining C_2H_5OH on the membrane surface, and air dried. A K 550 sputter coater was used to coat the outer surface of the membrane samples with a thin layer of gold under vacuum to provide electrical conductivity and to prevent the surface from being charged. The membranes were sputtered for 0.5 min with gold, and then the samples were examined under the electron microscope at potential of 10.0 kV. Using the same samples in the FESEM, the surface composition mapping and dispersion quality of TiO_2 particles on the membrane surface were examined using an Energy Dispersive X-ray (EDX) spectrometer (EDAX, USA).

Atomic Force Microscopy (AFM) Analysis. Atomic Force Microscopy (AFM), model XE-100 (Park Systems, USA), was employed to analyze the surface morphology and the roughness of the membranes. The measurement was carried out at atmospheric pressure and the membranes were dried at room temperature prior to surface analysis. Approximately 1 cm^2 of the prepared membrane was cut and affixed on the top of the scanner tube taped with carbon tape before being scanned to ensure that the sample was totally flattened. The membrane surface was then scanned with a laser beam reflected by the cantilever within a scanning area of 10 $\mu m \times 10\ \mu m$ based on the non-contact mode. The root mean square roughness (R_q) was recorded as the average of three measurements and was used as the evaluation parameter to compare the roughness of the membranes produced.

Adsorption Study

Adsorption of the HAs as model organic foulants and their binding kinetics onto the PVDF and PVDF–OH polymer surface was investigated using QCM-D. The polymers (with 5% PVDF/PVDF–OH and 95% DMAc) were spin-coated on quartz crystals (gold sensor) (14-mm diameter, $\sim$ 0.3-mm thickness). The tests were carried out in three steps: (i) deionized water flow for 5 minutes, (ii) HA solution flow for 1 h and (iii) deionized water flow for 1 h for hydraulic cleaning. Because the voids and pores of the freshly polymer coated quartz crystal (gold sensor) were filled during the experiment and gravely affected the experimental result, a water pre-adsorption study was first conducted using distilled water until a steady-state frequency (Δf) and energy dissipation (ΔD) were achieved to alleviate the impact of water adsorbed onto the film. During the adsorption test, 20 mg/L of the HA model solution prepared following the same procedure as mentioned in "Materials" section at pH 7 was charged into the flow modules at a constant cross-flow rate of 50.0 μL/min, and the weight changes were recorded by the measurement chamber.

For a rigid adsorbed layer (i.e., negligible energy dissipation, ΔD), changes in the frequency are primarily proportional to the mass uptake or release at the sensor surface as described by the Sauerbrey equation:[24]

$$\Delta f = -\frac{2{f_O}^2}{A\sqrt{\rho_q \mu_q}}\Delta m \tag{3}$$

where Δf is the change in frequency (Hz), Δm is the change in mass adsorbed (kg), f_O is the resonant frequency (Hz) of the crystal sensor, A is the piezoelectrically active crystal area (m^2), and ρ_q and μ_q are the density (kg/m^3) and shear modulus (Pa) of quartz.

Changes in the energy dissipation factor (ΔD) are related primarily to the viscoelasticity (softness). The softness, in turn, is often related to structural changes of the film adhering at the sensor surface. For viscoelastic layers that exhibit high energy dissipation (ΔD), the vibrations amplify the shear acoustic wave such that Δf is not directly proportional to Δm. A viscoelectric model was used to fit the Δf and ΔD data simultaneously to determine the density (ρ_1), thickness (d_1), shear elastic modulus (μ_1), and viscosity (η_1) of the adsorbed layer.[25–27] All adsorption study experiments were performed at 25°C.

The adsorption study of the HA model solution was continued for 1 h. Hydraulic cleaning was then conducted, and the polymer was washed in the same cross-flow manner with pure distilled water across the polymer surface continuously for another

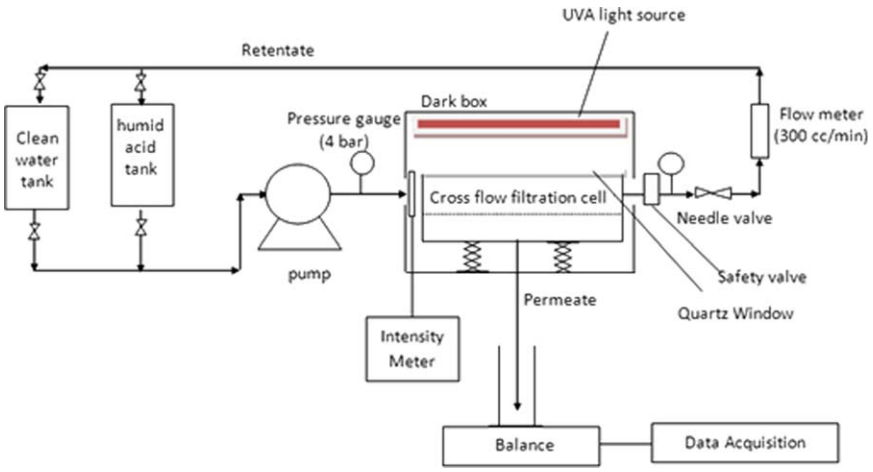

Figure 2. Schematic diagram of membrane cross-flow filtration rig. [Color figure can be viewed in the online issue, which is available at wileyonlinelibrary.com.]

1 h to remove loosely bonded HA, which determined the reversible fouling recovery.

Membrane Performance Evaluation

A laboratory bench scale cross-flow recirculation unit was used to study the permeation flux, antifouling, defouling and UV-cleaning properties of the neat PVDF membrane, PVDF/TiO_2 MMM and PVDF–OH/TiO_2 MMM. The schematic diagram of the experimental set-up for the cross-flow permeation unit is displayed in Figure 2. The rig consists mainly of a membrane cross-flow filtration cell, feed reservoir (HA tank and clean water tank), peristaltic pump, flow meter for measuring flow rate, balance with data acquisition system for measuring filtrate flow, pressure gauge to show the equilibrium pressure, and Philip UV-A light (Actinic BL TL-K 40 W/10-R), which emits long wave UV-A radiation in the 350–400 nm range to provide near-UV radiation. An intensity meter (Sglux, sensor monitor 5.0) was used to measure the UV light intensity. The produced flat sheet membrane was cut into a rectangular shape, laid on top of the membrane holder in a custom-designed transparent rectangular membrane test cell with a size of 7.5 cm × 9.6 cm (effective membrane filtration area of 72.0 cm^2, excluding the area covered by the O-ring) and was tightened by a rubber O-ring.

The experiment in this study included five successive steps using the same system but different experimental conditions. Fresh polymeric membranes were first compacted using pure distilled water at a constant pressure of 0.5 bar for 4 h until a steady-state flux was achieved. Fresh distilled water was then re-circulated at a constant cross-flow rate per unit projection area of 0.04 L/min using the peristaltic pump (Hydra-Cell, Wanner International).

The pure water flux (PWF) was determined every minute based on weight differences measured directly by the electronic balance connected to a data acquisition system (AND Super Hybrid Sensor, Model: Fx-3000i, A & D Company, Limited) over the permeation time.

$$F = \frac{V}{At} \tag{4}$$

where F is the PWF ($L/m^2{\cdot}h$), V is the permeate volume (L), A is the membrane effective surface area (m^2), and t is the permeation time (h).

The fouling experiment was performed for 12 h using 2 mg/L HA with 1 mM $CaCl_2$ as a model solution to simulate the organic matter in natural waters at ambient temperature (25°C) and at pH 7, according to the previously outlined procedure ("Materials" section). Fresh HA solution was added every 2 h to maintain a constant concentration.

The fouling tendency of the membranes was evaluated based on the relative flux reduction (RFR) which indicates the fouling propensity of the membrane. The RFR was calculated as follows:

$$\mathrm{RFR}(\%) = \left(1 - \frac{J_P}{J_{W1}}\right) \times 100\% \tag{5}$$

where J_P is the solution permeate flux ($L/m^2{\cdot}h$) and J_{W1} is the initial PWF ($L/m^2{\cdot}h$). Generally, the lower the RFR value, the better the antifouling properties of the membrane. Fouling can be quantified by the resistance to the flux due to pore blocking or the formation of a gel layer on the membrane surface.

After the HA solution was continuously filtered for 12 h, hydraulic cleaning was introduced in the cross-flow manner using distilled water for another 4 h to determine the flux recovery of the membranes. The flux recovery ratio (FRR) can be calculated from the water flux after hydraulic cleaning

$$\mathrm{FRR}(\%) = \left(\frac{J_{W2}}{J_{W1}}\right) \times 100\% \tag{6}$$

where J_{W2} is the PWF after washing ($L/m^2{\cdot}h$) and J_{W1} is the initial PWF ($L/m^2{\cdot}h$). Generally, a higher FRR (approaching unity) indicates better defouling properties of the membrane.

The photocatalytic degradation of HA was carried out by directly illuminating the corresponding fouled membrane for 3 h with a 40 W UVA lamp, Actinic BL TL/TL-D/T5 (Philips, Germany) with a light intensity at the membrane surface of 1.53 mW/cm^2 without water flow to activate the self-cleaning properties of the embedded TiO_2 NPs on the MMM surface.

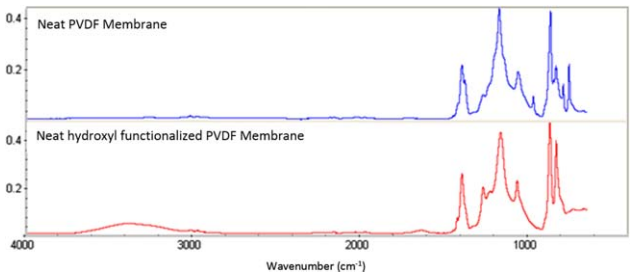

Figure 3. FTIR spectra of the neat PVDF polymer and PVDF–OH polymer. [Color figure can be viewed in the online issue, which is available at wileyonlinelibrary.com.]

Next, the water permeability test was conducted for 4 h, and the flux of the membrane was measured again. The same process was repeated twice to determine the UV irradiation time and the degree of HA degradation. For comparison purposes, this series of tests was also performed on the neat PVDF membrane as a control.

The irreversible flux recovery ratio [IFRR (UV)] from two cycles of photocatalytic degradation (3 h per cycle) was obtained by calculating the ratio of water permeability after UV irradiation to water permeability before irradiation:

$$\mathrm{IFRR(UV)(\%)} = \left(\frac{J_{W3} - J_{W2}}{J_{W2}}\right) \times 100\% \qquad (7)$$

where J_{W3} is the recovery water flux after irradiation with 6 h of UV light (L/m^2·h) and J_{W2} is the PWF after washing with distilled water (L/m^2·h) without UV light.

RESULTS AND DISCUSSION

Chemical Modification of PVDF

The FTIR spectra of the PVDF and PVDF–OH polymer are shown in Figure 3. As depicted in Figure 3, a strong characteristic peak for the PVDF–OH polymer FTIR spectra that corresponds to the O—H stretching was observed in a broad band around 3500–3000 cm^{-1}. The presence of the higher O—H stretching absorbance of the PVDF–OH polymer means that the PVDF–OH polymer could primarily give higher hydrophilicity to the PVDF–OH membrane and is therefore expected to have a higher water flux.

Adsorption Study on the Pristine PVDF and PVDF–OH Membranes

To prove that the PVDF–OH polymer with more hydroxyl groups has better antifouling properties, a QCM-D adsorption study of 20 mg/L HA solution on the neat PVDF membrane and PVDF–OH membrane was carried out. Figure 4 clearly reveals that the frequency change (Δf) of the PVDF–OH membrane related primarily to the change in mass adsorbed (Δm) was lower than the frequency change of the neat PVDF membrane. In other words, the rate and extent of membrane fouling of the PVDF membrane are higher than the rate and extent of membrane fouling of the PVDF–OH membrane. The thickness of the fouled PVDF–OH membrane is more readily reduced compared to the PVDF membrane.

The change in energy dissipation (ΔD) is defined as the loss of energy per oscillation period divided by the total energy stored in the system that is related to the film viscoelastic property (softness). With more foulant adhering on the PVDF membrane film, the structure of the film will change from rigid to a thicker and softer adsorbed layer, thus dampening the oscillation of the sensor. The damping of the oscillation of the sensor is revealed by exhibiting a high ΔD. Upon cleaning with pure water, the PVDF–OH membrane exhibited a lower ΔD value compared to the unchanged ΔD value of the neat membrane. The lower ΔD means that the adsorbed layer becomes more rigid, indicating that the water-coupled elongated HA layer could be removed easily from the PVDF–OH just by hydraulic cleaning.

Physical Properties of the PVDF/TiO_2 MMM

Figure 5 shows the FESEM top surface images and EDX mapping of the PVDF/TiO_2 MMM and PVDF–OH/TiO_2 MMM prepared using DMAc as a solvent and immersed in 0.01 g/L P25 colloid suspension. As shown in the images, the PVDF–OH/TiO_2 MMM was more favorable for producing smaller surface particles compared to the system using the pristine PVDF polymer. The EDX analysis was applied to further confirm the distribution of TiO_2 NPs on the top surface of the PVDF/TiO_2 MMM and PVDF–OH/TiO_2 MMM. The EDX mapping analysis demonstrated that the PVDF–OH/TiO_2 MMM has a fairly good

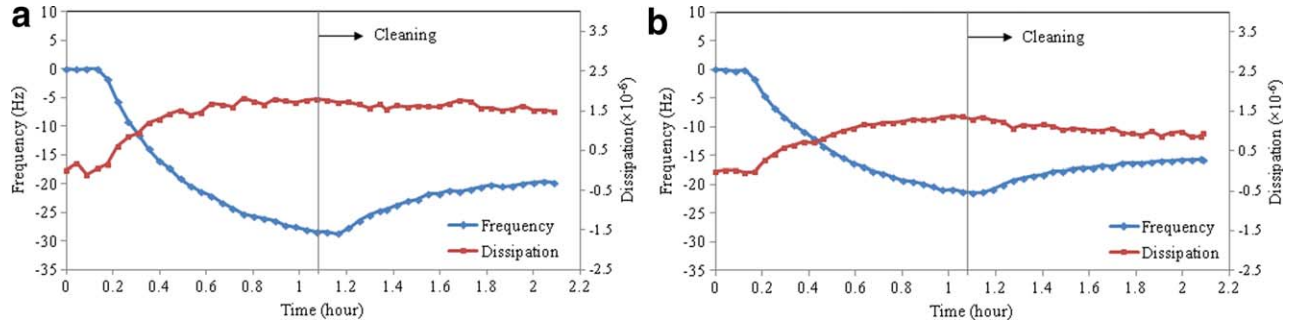

Figure 4. Dissipation change (ΔD) and frequency change (Δf) of (a) neat PVDF membrane and (b) neat PVDF–OH membrane during three cycles of cross-flow process: deionized water flow for 5 minutes, HA solution flow for 1 h, deionized water flow of hydraulic cleaning for 1 h. Casting solution composition: PVDF/DMAc = 5: 95. Operation conditions during the experiment: [HA] = 20 mg/L; [Ca^{2+}] = 1 mM (as $CaCl_2$); pH 7.0; temperature = 25 ± 1°C; constant cross-flow rate = 50.0 μL/min. [Color figure can be viewed in the online issue, which is available at wileyonlinelibrary.com.]

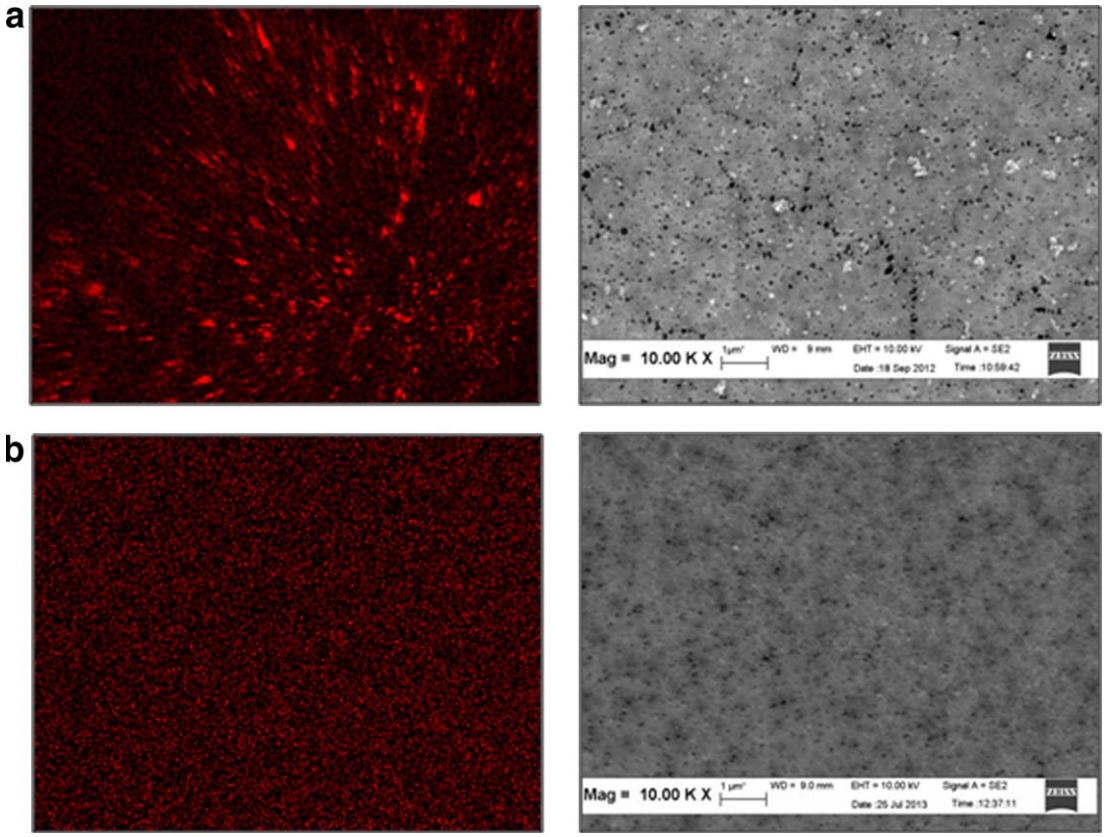

Figure 5. FESEM micrographs and EDX top surface mapping of the (a) PVDF/TiO_2 MMM and (b) PVDF–OH/TiO_2 MMM fabricated using DMAc as a solvent by immersing in a 0.01 g/L P25 TiO_2 coagulation bath. [Color figure can be viewed in the online issue, which is available at wileyonlinelibrary.com.]

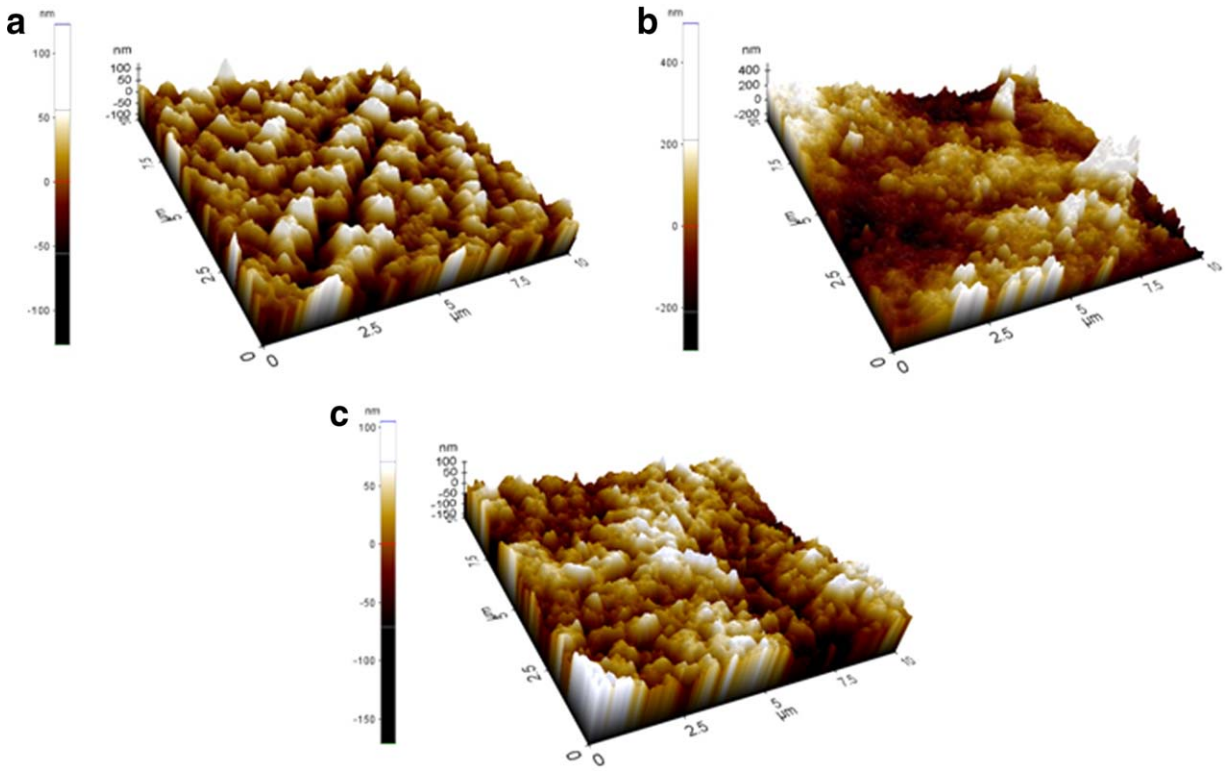

Figure 6. AFM three-dimensional surface micrographs of the (a) neat PVDF membrane, (b) PVDF/TiO_2 MMM and (c) PVDF–OH/TiO_2 MMM. [Color figure can be viewed in the online issue, which is available at wileyonlinelibrary.com.]

Table I. Surface Parameters for the Neat PVDF Membrane, PVDF/TiO_2 MMM, and PVDF-OH/TiO_2 MMM Fabricated Using DMAc as a Solvent Immersed in 0.01 g/L of TiO_2 Colloid Suspension

Membrane	R_q (nm)	Surface area ratio (%)
PVDF	20.7	1.8
PVDF/TiO_2	107.4	15.1
PVDF-OH/TiO_2	36.1	4.5

Note: The root mean square value of Z data (R_q) is the standard deviation of the Z values within the given area.

particle distribution on the membrane surface compared to the PVDF/TiO_2 MMM. The lesser degree of TiO_2 clustering for the PVDF–OH/TiO_2 MMM is most likely attributed to the relatively lower surface tension between the particles and the hydrophilized membrane matrix contributed by the hydroxyl group.

AFM was employed to further analyze the surface morphology and the roughness of the neat PVDF membrane, PVDF/TiO_2 MMM and PVDF–OH/TiO_2 MMM. Figure 6 shows three-dimensional AFM images of membrane surfaces at a scan size of 10 μm × 10 μm. In these images, the brightest area represents the highest point of the membrane surface, and the dark regions indicate the valleys or membrane pores. For the PVDF/TiO_2 MMM, the surface morphology was greatly changed by the clustering effect of TiO_2 NPs assembled on the PVDF membrane, whereas the PVDF–OH/TiO_2 MMM shows a surface roughness quite similar to that of the pristine membrane.

The surface roughness parameters of the membranes, expressed in terms of the root mean square of the Z data (R_q) and the surface area ratio (%), were calculated using the XE Image Processing Program Version 1.7.6, and the results are presented in Table I. Table I shows that the roughness parameters of the PVDF–OH/TiO_2 MMM were apparently lower than the roughness parameters of the PVDF/TiO_2 MMM and closer to those of the neat PVDF membrane. At equal TiO_2 concentrations, the better dispersion of TiO_2 within the PVDF–OH polymer matrix gave a higher number of surface TiO_2 clusters (particles) compared to the PVDF polymer matrix. In addition, the coarser membrane traps impurities from water to reduce the surface

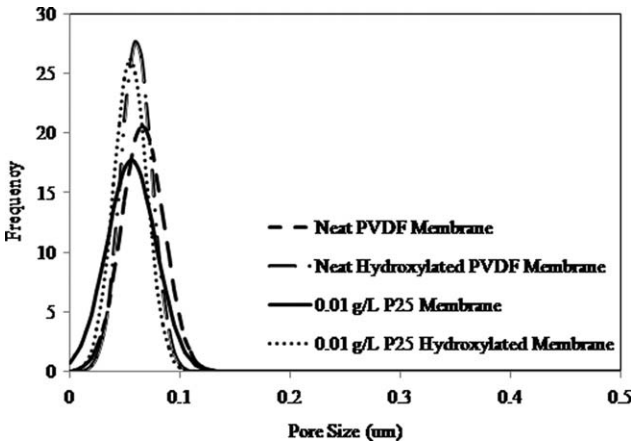

Figure 7. The pore size distribution of membranes.

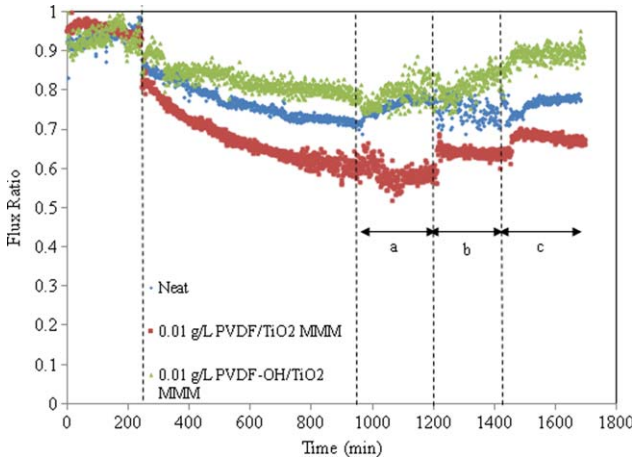

Figure 8. Effect of the hydroxyl-functionalized P25 MMM on antifouling potential during five cycles of the cross-flow filtration process: PWF for 4 h, HA solution filtration for 12 h, hydraulic cleaning PWF for 4 h, water flux for 4 h after 3 h of UV irradiation and water flux for 4 h after a 2nd round of 3 h UV irradiation. Operation conditions during the experiment: [HA] = 2 mg/L; [Ca^{2+}] = 1 mM (as $CaCl_2$); pH 7.0; temperature = 25 ± 1°C; cross-flow velocity = 4.0 L/h, operating pressure = 0.5 bar; light intensity = 1.53 mW/cm^2. (a) hydraulic cleaning, (b) hydraulic cleaning after 3 h of UV irradiation, [c] hydraulic cleaning after another subsequent 3 h of UV irradiation. [Color figure can be viewed in the online issue, which is available at wileyonlinelibrary.com.]

energy much more easily. Therefore, the smoother surface of the PVDF–OH/TiO_2 MMM with less surface roughness is expected to have a low fouling tendency.

Figure 7 shows that the produced membranes have pore size distribution that could be classified into two categories. In overall, the hydroxylated PVDF membranes have narrower pore size distribution compared to the neat PVDF membrane. However, these membranes have similar average pore size around 0.06 μm. It is important to note that, neither membranes showed significant pore size changes upon addition of P25 NPs via *in-situ* colloidal precipitation method.[18]

Antifouling and UV-Cleaning Potential of the Membrane

Antifouling Properties of the Membranes (RFR). To determine the performance of the PVDF–OH/TiO_2 MMM, a series of cyclic filtration tests on the antifouling, defouling and UV-cleaning properties was conducted, and the flux data for these successive filtrations are illustrated in Figure 8 and Table II. The flux data are presented in terms of normalized flux (J/J_O), which is the instantaneous flux over the initial water flux. The discontinuity of each curve was due to the intermittent operation carried out throughout the experiment. For PWF filtration, the normalized fluxes were relatively constant subsequent to 4 h of operation. Considering that groundwater frequently has a hardness (mainly calcium and magnesium) above 300 mg/L as $CaCO_3$,[28] calcium was added to the feed solution to explore its effects on fouling behavior. Although HA molecules alone could not be effectively adsorbed onto the TiO_2 particles or onto the membrane matrix at pH 7.0, the presence of calcium ions in the solution significantly enhanced the HA adsorption onto the surface of TiO_2.[20,29] With the presence of the divalent cation (Ca^{2+}) in the HA solution, the

Table II. The Water Flux Recovery and Cleaning Property of the Neat PVDF Membrane, PVDF/TiO_2 MMM, and PVDF-OH/TiO_2 MMM Fabricated Using DMAc as Solvent Immersed in 0.01 g/L TiO_2 Colloid Suspension

Membrane	TiO_2 concentration (g/L)	Contact angle (°)	Rejection (%)	RFR	FRR	IFRR (UV)
PVDF	-	66.9 ± 1.1	97.92 ± 0.63	24.24	82.03	0.10
PVDF/TiO_2	0.010	75.2 ± 0.5	98.73 ± 0.19	36.07	61.89	16.56
PVDF-OH/TiO_2	0.010	74.4 ± 0.7	95.83 ± 1.59	15.24	87.32	11.15

HA molecules became a coiled and spherical cohesive mass.[30,31] This effect is due to the electrostatic shielding of the HA carboxyl functional groups[32] and consequently results in a decrease of the electrostatic repulsion between HA molecules to form bigger molecules due to coagulation and particle precipitation.[30,33] Yuan and Zdyney[33] reported that the reaggregation of HA due to Ca^{2+} precipitation changed the apparent molecular distribution of HA, i.e., the portion of HA with molecular weight greater than 300 kD increased from only 1% for the fresh solution to 9% for the solution in the presence of 1 m*M* $CaCl_2$. Such an adsorbed layer caused a sharp drop in the flux, even in the first few minutes of operation.

The initial water flux (J_o) for the neat PVDF, PVDF/TiO_2 and PVDF–OH/TiO_2 membranes are 37.4, 37.7, and 25.0 L/hr.m^2, respectively. The flux data showed that hydroxylation of PVDF did narrow down the pores as supported by previous pore size data which cause certain degree of flux declination. The rejection of the membrane seems decreased slightly for PVDF–OH/TiO_2 membrane in despite of its smaller pore size as shown in Table II. It is important to note that the pore size of the membrane is relatively large (60 nm) compared to the isolate HA, in this case the buildup of cake layer do help to enhance the rejection of the membranes. Upon membrane hydroxylation, the HA deposition on the membrane surface was reduced which resulted in poorer observed rejection.

The HA fouling tendency was revealed clearly by the considerable flux decline in Figure 8 with RFR values of 24.24%, 36.07%, and 15.24% for the neat PVDF membrane, PVDF/TiO_2 MMM and PVDF–OH/TiO_2 MMM, respectively, after 12 h of HA filtration (the end of HA fouling). Visual observation revealed that the membrane surface was covered with a thin dark brown deposit layer (gel formation) at the end of the filtration, confirming the existence of the fouling layer. The cross-sectional images (Figure 9) of the membranes (PVDF, PVDF/TiO_2, and PVDF–OH/TiO_2) shows that the the neat PVDF membrane has the thickest foulant layer followed by the PVDF/TiO_2 and PVDF–OH/TiO_2. This phenomenon proved that membrane hydrophilization could indeed minimize the fouling tendency of HA. This observation was also in accordance to the previous observation that explain why PVDF–OH/TiO_2 had poorer HA rejection because of its thinner layer.

The membrane fouling phenomenon could be influenced by hydrodynamic conditions, such as permeation drag and back transport, and chemical interaction between foulants and membranes.[34] To relate the hydrophilicity to the antifouling property, the membranes were tested under similar hydrodynamic conditions. Hence, the different fouling behavior could be attributed to the different physiochemical properties of the membranes due to NPs entrapment. Theoretically, the incorporation of hydrophilic TiO_2 into the PVDF membrane matrix could reduce the fouling propensity of the membrane[35–37] due to the higher affinity of TiO_2 toward water. As reported in the literature, the antifouling properties of TiO_2 NPs were attributed to the water-shielding effect by the hydrophilic hydroxyl groups on the membrane surface.[38,39] However, the PVDF/TiO_2 MMM, which exhibited a high surface roughness problem, superseded the hydrophilicity effect of the membrane and eventually led to an increase in fouling tendency (higher RFR) compared with the neat PVDF membrane. As can be seen from Table II, even though the PVDF–OH/TiO_2 membrane has lower contact angle compared to PVDF/TiO_2 membrane, however, both MMM membranes show higher contact angle compared to the neat membrane. This observation showed that surface roughness did play an important role in lowering the surface energy thus increasing the contact angle. Cao *et al.*[5] found that the membrane roughness was the most influential factor on the membrane antifouling capability under the same operating conditions. Coarser membranes can much more easily absorb foulants from water in the valleys of the membrane compared to smoother membrane surfaces.[5,40–42]

In the PVDF–OH/TiO_2 MMM system, in which the particle distribution was enhanced, the HA fouling propensity of the membrane was greatly reduced, as shown by the lower RFR value compared to the neat PVDF membrane and unmodified PVDF/TiO_2 MMM. This finding shows that the fine and uniformly distributed NP membrane with lower surface roughness and higher surface energy was responsible for its antifouling properties. This finding was in line with the work of Cao *et al.* (2006), who claimed that compared to the rutile TiO_2 NPs (average diameter ~ 30 nm), anatase TiO_2 NPs with a smaller diameter (~10 nm) are reported to have better antifouling properties.[5]

Hydraulic Cleaning Properties of Membranes (FRR). Membrane fouling can be reversible or irreversible. Reversible fouling in this study resulted from the loose attachment of HA on the membrane surface, which could be removed by simple hydraulic cleaning. In contrast, irreversible fouling was caused by the strong adsorption of HA molecules onto the surface or the entrapment of HA molecules in pores which cannot be removed by hydraulic cleaning. In this case, membrane cleaning was studied by scouring the membrane surface with pure distilled water. Cleaning was performed by recirculating pure water at 0.04 L/min for 4 h. As shown in Figure 8, a significant increment in flux was found after the membrane was washed with pure distilled water. The permeation flux recovery was expressed in terms of the FRR. The water

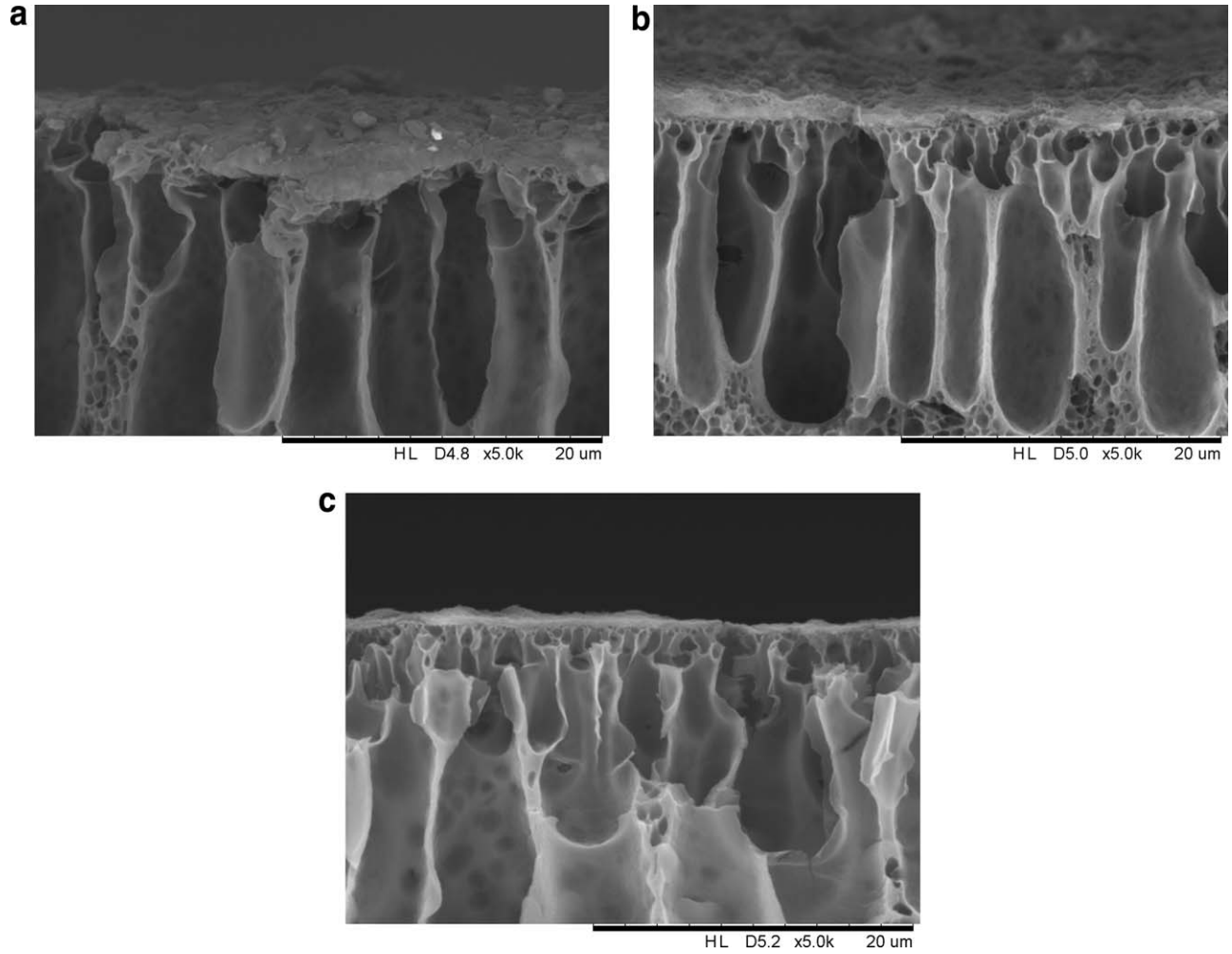

Figure 9. Cross-sectional images of the HA fouling layer on different membranes (a) Neat PVDF membrane, (b) PVDF/TiO_2 MMM (c) PVDF–OH/TiO_2 MMM.

flux can be recovered up to 82.03%, 61.89% and 87.32% for the neat PVDF membrane, PVDF/TiO_2 MMM and PVDF–OH/TiO_2 MMM, respectively. This observation indicated that the flux decline caused by HA was mostly reversible, most likely due to the surface reversible deposition that could be improved significantly using hydraulic force.

Again, the recovery of the PVDF/TiO_2 MMM flux appeared to have a lower FRR than the neat PVDF membrane. This observation further supports the suggestion that irregular surface roughness promoted the adsorption of HA molecules that are difficult to remove due to the zero shear near the surface. The PVDF–OH/TiO_2 MMM was likely to shown an extraordinary advantage for membrane defouling properties. This quality was further enhanced by the uniform roughness of the membrane surface due to the trapping of air in the cavities between the drop and the hierarchical nodular structure of the membrane surface (wetting resistance), which could easily repel the water by rolling off the water with anchoring HA.[43]

Self-Cleaning Ability of Intermittently UV-Irradiated Membranes [IFRR (UV)]. Photocatalytic degradation of the adsorbed HA was performed after physical cleaning by irradiating the membrane surfaces twice (3 h each) with a UV-A lamp at a light intensity of 1.53 mW/cm^2.

After irradiating with UV light, the fouled membrane, which was initially dark brown in color gradually changed to light brown and almost yellow when photocatalytic oxidation was employed, while the color of the fouled neat PVDF membrane remained the same. Figure 8 shows that the filtration flux of the MMM was effectively enhanced after UV irradiation. These results prove that the effect of photocatalysis on the MMMs did provide additional cleaning properties. During photocatalytic degradation, TiO_2 particles on the MMM surface interact with UV light to generate electrons (e^-) and holes (h^+). The photogenerated holes trap H_2O or O_2 to yield H^+ and highly active HO• radicals, which are an effective oxidation agent for destroying HAs. Generally, HO• attacks the HA molecule through hydroxyl addition or hydrogen extraction. Meanwhile, dissolved oxygen (DO) in water can capture electrons and produce O_2^-, which reacts with HA or HA intermediates. DO can further form •OH by protonation, which results in the degradation of HA.

IFRR (UV) values of 0.10, 16.56 and 11.15 were recorded for the neat PVDF membrane, PVDF/TiO_2 MMM and PVDF–OH/TiO_2

MMM, respectively. Table II shows that the IFRR (UV) obviously had an insignificant effect on the neat membrane, as the UV light alone failed to degrade HA deposited on the membrane surface. Because photocatalytic activity of the MMM is contributed by the embedded TiO_2 NPs, it is reasonable to find that the PVDF–OH/TiO_2 MMM also showed enhanced photocatalytic activity.

The flux changes from 37.7 to 25.6 L/h.m^2 and 25 to 22.5 L/h.m^2 for PVDF–TiO_2 and hydroxylated PVDF–OH/TiO_2, respectively. These results show that even though the overall flux of PVDF–TiO_2 membrane is still higher due to the bigger pore size, for long term operation, hydroxylated PVDF–OH/TiO_2 has better antifouling properties. The amalgamation of superior antifouling, defouling and UV-cleaning ability of the PVDF–OH/TiO_2 MMM prepared using the *in-situ* colloidal precipitation method was therefore attractive for longer operational lifetimes that could reduce its operating costs.

CONCLUSIONS

The fine and well-distributed TiO_2 dispersions with a low tendency for aggregation on the membrane polymeric matrix were found to have significant effects on the membrane antifouling and defouling properties. The antifouling and defouling properties were attributed to their reduced surface roughness as well as to their increasing surface energy. This finding was manifested through the improved RFR and FRR values of the PVDF–OH/TiO_2 MMM compared to the PVDF/TiO_2 MMM and neat membrane.

The ultimate advantage of incorporating TiO_2 NPs into the membrane matrix for self-cleaning properties was evaluated by degrading the HA adsorbed on the membrane surface under mild UV light irradiation. Photocatalytic oxidation was found to be an effective process for degrading permanently fouled HA by breaking the hydrophobic and electrostatic interactions between HA and the membrane and thus increase the membrane cleaning efficiency. P25 TiO_2, with mixed 25% rutile and 75% anatase crystallinity, was proven to produce superior UV-cleaning properties towards the PVDF/TiO_2 MMM. However, the photodegradation property of the PVDF/TiO_2 MMM was complicated by its rough surface. This problem can be solved by hydroxylizing the polymer matrix to improve the TiO_2 dispersion. The PVDF–OH/TiO_2 MMM containing the well-dispersed TiO_2 NPs with a large surface-to-volume ratio was considered to be an attractive membrane that promises significant amalgamation of the applications to antifouling, defouling and UV-cleaning (self-cleaning) capacity.

ACKNOWLEDGMENTS

The authors thank the sponsors of this project for their financial support, namely the Universiti Sains Malaysia (USM) Research University Grant (1001/PJKIMIA/811172), MOSTI eSciencefund (305/PJKIMIA/6013604), USM Fellowship and the USM Membrane Science and Technology Cluster.

REFERENCES

1. Wu, L.; Sun, J.; Wang, Q. *J. Membr Sci.* **2006**, *285*, 290.
2. Sauguet, L.; Boyer, C.; Ameduri, B.; Boutevin, B. *Macromolecules* **2006**, *39*, 9087.
3. Yan, L.; Hong, S.; Li, M. L.; Li, Y. S. *Sep. Purif. Tech.* **2009**, 66, 347.
4. Ji-xiang, Y.; Wen-xin, S.; Shui-li, Y.; Yan, L. *Desalination* **2009**, *239*, 29.
5. Cao, X.; Ma, J.; Shi, X.; Ren, Z. *Appl. Surf. Sci.* **2006**, *253*, 2003.
6. Chin, S. S.; Chiang, K.; Fane, A. G. *J. Membr. Sci.* **2006**, *275*, 202.
7. Yuliwati, E.; Ismail, A. F. *Desalination* **2011**, *273*, 226.
8. Han, L.-F.; Xu, Z.-L.; Yu, L.-Y.; Wei, Y.-M.; Cao, Y. *Iranian Polym. J.* **2010**, 19, 553.
9. Kim, J.; Van der Bruggen, B. *Environ. Pollut.* **2010**, *158*, 2335.
10. Li, J.-B.; Zhu, J.-W.; Zheng, M.-S. *J. Appl. Polym. Sci.* **2007**, *103*, 3623.
11. Li, J.-F.; Xu, Z.-L.; Yang, H.; Yu, L.-Y.; Liu, M. *Appl. Surf. Sci.* **2009**, *255*, 4725.
12. Li, J.-H.; Xu, Y.-Y.; Zhu, L.-P.; Wang, J.-H.; Du, C.-H. *J. Membr. Sci.* **2009**, *326*, 659.
13. He, P.; Zhao, A. C. *Acromolecule Aviso.* **2001**, *2*, 74.
14. Zheng-ping, F.; Yu-zhen, X.; Cheng-wei, X. *J. Mater. Sci. Eng.* **2003**, *21*, 279.
15. Bae, T.-H.; Tak, T.-M. *J. Membr. Sci.* **2005**, *249*, 1.
16. Yu, L.-Y.; Shen, H.-M.; Xu, Z.-L. *J. Appl. Polym. Sci.* **2009**, *113*, 1763.
17. Rahimpour, A.; Madaeni, S. S.; Taheri, A. H.; Mansourpanah, Y. *J. Membr. Sci.* **2008**, *313*, 158.
18. Teow, Y. H.; Ahmad, A. L.; Lim, J. K.; Ooi, B. S. *Desalination* **2012**, *295*, 61.
19. Teow, Y. H.; Ahmad, A. L.; Ooi, B. S. *Glob. J. Environ. Sci. Technol.* **2013**, *2*, 1.
20. Teow, Y. H.; Ahmad, A. L.; Lim, J. K.; Ooi, B. S. *J. Appl. Polym. Sci.* **2012**, *128*, 3184.
21. Teow, Y. H.; Ooi, B. S.; Ahmad, A. L.; Lim, J. K. *Inter. J. Chem. Eng. Appl.* **2012**, *3*, 374.
22. Auvinen, S.; Alatalo, M.; Haario, H.; Vartiainen, E.; Jalava, J.-P.; Lamminmäki, R.-J. *J. Phys. Chem. C* **2013**, *117*, 3503.
23. Devore, J. R. *J. The Opt. Soc. of Am.* **1951**, *41*.
24. Sauerbrey, G. *Zeitschrift für Physik* **1959**, *155*, 206.
25. Voinova, M. V.e.a. *Phys. Script.* **1999**, *59*, 391.
26. Diethelm, J. *Macromol. Chem. Phys.* **1999**, *200*, 501.
27. Bandey, H. L.; Hillman, A. R.; Brown, M. J.; Martin, S. J. *Faraday Disc.* **1997**, *107*, 105.
28. Wang, Z.; Zhao, Y.; Wang, J.; Wang, S. *Desalination* **2005**, *178*, 171.
29. Srisurichan, S.; Jiraratananon, R.; Fane, A. G. *Desalination* **2005**, *174*, 63.
30. Schäfer, A. I. Natural organics removal using membranes In UNESCO Centre for Membrane Science and Technology, University of New South Wales: Sydney, **1999**.
31. Hong, S.; Elimelech, M. *J. Membr. Sci.* **1997**, *132*, 159.
32. Jucker, C.; Clark, M. M. *J. Membr. Sci.* **1994**, *97*, 37.

33. Yuan, W.; Zydney, A. L. *J. Membr. Sci.* **1999**, *157*, 1.
34. Maximous, N.; Nakhla, G.; Wan, W. *J. Membr. Sci.* **2009**, *339*, 93.
35. Bae, T.-H.; Kim, I.-C.; Tak, T.-M. *J. Membr. Sci.* **2006**, *275*, 1
36. Bae, T.-H.; Tak, T.-M. *J. Membr. Sci.* **2005**, *266*, 1.
37. Kim, S. H.; Kwak, S.-Y.; Sohn, B.-H.; Park, T. H. *J. Membr. Sci.* **2003**, *211*, 157.
38. Madaeni, S. S.; Ghaemi, N. *J. Membr. Sci.* **2007**, *303*, 221.
39. Madaeni, S. S.; Ghaemi, N.; Alizadeh, A.; Joshaghani, M. *Appl. Surf. Sci.* **2011**, *257*, 6175.
40. Idris, A.; Mat Zain, N.; Noordin, M. Y. *Desalination* **2007**, *207*, 324.
41. Boussu, K.; Van der Bruggen, B.; Volodin, A.; Van Haesendonck, C.; Delcour, J. A.; Van der Meeren, P.; Vandecasteele, C. *Desalination* **2006**, *191*, 245.
42. Vrijenhoek, E. M.; Hong, S.; Elimelech, M. *J. Membr. Sci.* **2001**, *188*, 115.
43. Zhao, X.; Chen, W.; Su, Y.; Zhu, W.; Peng, J.; Jiang, Z.; Kong, L.; Li, Y.; Liu, J. *J. Membr. Sci.* **2013**, *441*, 93.